Structural and mechanistic insight into Holliday-junction dissolution by Topoisomerase III and RMI1

Bocquet, Nicolas ; Bizard, Anna H ; Abdulrahman, Wassim ; Larsen, Nicolai B ; Faty, Mahamadou ; Cavadini, Simone ; Bunker, Richard D ; Kowalczykowski, Stephen C ; Cejka, Petr ; Hickson, Ian D ; Thomä, Nicolas H

Abstract: Repair of DNA double-strand breaks via homologous recombination can produce double Holliday junctions (dHJs) that require enzymatic separation. Topoisomerase III (TopIII) together with RMI1 disentangles the final hemicatenane intermediate obtained once dHJs have converged. How binding of RMI1 to TopIII influences it to behave as a hemicatenane dissolvase, rather than as an enzyme that relaxes DNA topology, is unknown. Here, we present the crystal structure of human TopIII complexed to the first oligonucleotide-binding domain (OB fold) of RMI1. TopIII assumes a toroidal type 1A topoisomerase fold. RMI1 attaches to the edge of the gate in TopIII through which DNA passes. RMI1 projects a 23-residue loop into the TopIII gate, thereby influencing the dynamics of its opening and closing. Our results provide a mechanistic rationale for how RMI1 stabilizes TopIII -gate opening to enable dissolution and illustrate how binding partners modulate topoisomerase function.

DOI: https://doi.org/10.1038/nsmb.2775

Structure of human topoisomerase IIIα in complex with RMI1 $OB_{N\text{-}Term}$

Mechanistic insight into RMI1 mediated decatenation

Nicolas Bocquet[1], Mahamadou Faty[1], Wassim Abdulrahman[1], Anna Bizard[2], Simone Cavadini[1], Richard Bunker[1], Heinz Gut[1], Henning Stahlberg[3], Steve Kowalczykowski[4], Petr Cejka[4,5], Ian David Hickson[2] & Nicolas Thomä[1].

To whom correspondence should be addressed: nicolas.thoma@fmi.ch

1. Friedrich Miescher Institute for Biomedical Research, Maulbererstrasse 66, CH-4058 Basel, Switzerland

2. Department of Cellular and Molecular Medicine, University of Copenhagen, Panum Institute, Building 18.1, Blegdamsvej 3B, 2200 Copenhagen N, Denmark

3. Center for Cellular Imaging and Nano Analytics (C-CINA), Biozentrum, University of Basel, Mattenstrasse 26, CH-4058 Basel, Switzerland

4. Department of Microbiology, University of California, Davis, One Shields Ave, Davis, CA 95616-8665 USA.

5. Present address: Institute of Molecular Cancer Research, University of Zurich Winterthurerstrasse 190, 8057 Zurich, Switzerland

List of abbreviations

CAP	Catabolite Activator Protein
C-strand	Cut Strand
dHJ	Double Holliday junction
DSB	Double Strand Break
dsDNA	Double strand DNA
EM	Electronic Microscopy
HR	Homologous recombination
LOH	Loss Of Heterozigocity
MMS	Methyl MethaneSulfonate
OB	Oligonucleotide Binding
RMI1	Human RecQ Mediated genome Instability 1
Rmi1	yeast RecQ Mediated genome Instability 1
RPA	Replication Protein A
SSB	Single Strand Binding protein
ssDNA	Single Strand DNA
TEV	Tobacco Etch Virus protease
Top3	Yeast or *E. coli* Topoisomerase 3
TopIIIα	Human Topoisomerase 3 alpha
T-strand	Transferred Strand

Abstract:

DNA double-strand breakage repair through homologous recombination produces double Holliday junctions (dHJ). The entangled DNA duplexes comprising the dHJ require enzymatic separation. While human topoisomerase TopIIIα serves in the final steps of dHJ decatenation, it requires assistance from RMI1 *in vitro* and *in vivo*. How RMI1 modulates TopIIIα structure and function hence converting the topoisomerase into a proficient decatenation enzyme remains unclear. Here we present the structure of human TopIIIα complexed to the first oligonucleotide binding (OB-fold) of RMI1 at 2.65 Å. TopIIIα assumes a canonical toroid topoisomerase 1A fold, with the RMI1 OB-fold attached to the top of the topoisomerase gate. RMI1 injects a 23-residue loop into the central cavity of TopIIIα, which directly influences the open/closure dynamics of the topoisomerase gate. We propose a decatenation mechanism whereby epitopes stabilizing gate opening favor decatenation relative to relaxation, demonstrating how topoisomerase function is modulated through its macromolecular environment.

Introduction

Homologous recombination (HR) is a central pathway in the repair of double-strand breaks and single-stranded gaps, and is required for maintaining and restarting stalled replication forks[1,2]. In HR, a homologous DNA sequence templates the repair of the damaged DNA strand. Following DNA synthesis and ligation, a double Holliday junction intermediate (dHJ) is produced, which interconnects two sister chromatids[3,4]. These dHJ intermediates are processed, either in a crossover, or non-crossover fashion[5-7]. Several nucleases are able to cleave the symmetrical Holliday junction, yielding an equal number of both products. The mitotic crossovers products, however, carry the risk of loss heterozygosity (LOH), a known driver of oncogenic transformation[8,9]. In mitotic cells LOH appears to be rare, contributing to only 2.5% of HR mediated double-strand breakage repair events[10]. Alternative pathways hence exist in cells biasing cellular HR completion towards non-crossover completion.

The DNA molecules within the dHJ intermediate are topologically linked. The disjunction of the entangled chromosomes can principally be accomplished through the duplex unwinding activity of a specific RecQ-type helicase, coupled to DNA strand unlinking by a type 1A topoisomerase. The interplay between RecQ helicase and topoisomerase, which is conserved in all kingdoms of life, exclusively generates non-crossover products[11]. In humans, TopIIIα works with BLM, a RecQ enzyme found mutated in the cancer predisposing Bloom syndrome, while in yeast it is Sgs1 that works in concert with Top3[12-14]. Whilst Sgs1/BLM and Top3/TopIIIα are required to process various topologically linked substrates[15,16], they act in concert with an additional essential component: Rmi1, in yeast[17,18], and the RMI1/RMI2 complex in human cells[19,20]. Together the RecQ helicase, Top3/IIIα and Rmi1/RMI1 form the minimal dHJ dissolvasome, loss or mutation of either component results in genomic instability in affected cells[18,21,22].

dHJ dissolution requires a branch migration step that collapses the two HJs into a hemi-catenane, followed by a dissolution step that unhooks the *hemi*-catenane intermediate into two separate DNA duplexes. In yeast, where the reaction has been biochemically dissected in detail[23-25],

convergence of the 2 HJs is driven by Sgs1 in an ATP dependent process. Top3 provides the enzymatic unlinking activity for helicase mediated dHJ migration, and unhooks the final *hemi*-catene[23].

TopIIIα is a member of the toroidal type 1A topoisomerases, which introduce single stranded nicks in one strand (cut strand: C-strand), allowing a second ssDNA strand to be transferred through the nick (transfer strand: T-strand). When T- and C-strands belong to separate duplexes, the outcome is decatenation, should they both belong to the same plectonemicaly linked duplex then relaxation is observed. The in/out-movement of DNA single-strand (T-strand) is made possible by a gate of intertwined β-sheets allowing reversible opening/closure of the toroid[26]. In this context, the C-strand is cut in a reversible, ATP independent, *trans*-esterification process giving rise to a 5'-tyrosine ssDNA intermediate, with the T-strand being moved through the nick[27]. Top3 and TopIIIα, in isolation, are relatively ineffective in relaxing negatively supercoiled plasmids, acting both as relatively poor decatenases. Effective decatenation is bestowed in the presence of RMI1, however, which works while inhibiting relaxase. In yeast, Rmi1 has been shown biochemically to stabilize the open conformation of the topoisomerase gate[23]. The molecular mechanism by which RMI1/Rmi1 modulates TopIIIα/3 function bestowing decatenation properties that allow dHJ dissolution has remained elusive.

We have set out to define how RMI1/Rmi1 modulates TopIIIα/3 function converting the complex into a single-strand specific decatenase using structural, biochemical and cellular biological approaches. We show *in vitro* and *in vivo,* that RMI1 contributes to decatenation process through donating of a decatenation loop *in trans*.

Results

Construct design underlying structural studies of the TopIIIα–RMI1complex

Human TopIIIα and yeast Top3 carry distinct sequence signatures that distinguish them from their prokaryotic Top3 counterparts (**Supplementary fig. 2,3** for sequence alignment and conservation). In the absence of structural information it is unclear to what extend the eukaryotic TopIIIα/Top3 decatenases diverge from their prokaryotic counterparts, and how RMI1 complements topoisomerase function conferring effective decatenase activity.

In an effort to address these questions we pursued the structure of the TopIIIα-RMI1 complex. Complexes from *S. cerevisiae*, *Xenopus laevis, Danio rerio*, *Mus musculus* and *Homo sapiens* were co-expressed, purified and subjected to crystallization trials. Crystals were obtained after 5-6 days for human TopIIIα (residues 1 to 753 following deletion of residues 753 to 1001) complexed to human RMI1 (DUF1767+OB_N: residue 1 to 219) (**fig. 1a, b, e)**,and belonged to space group $P4_12_12$ with one complex in the asymmetric unit (**Supplementary fig. 5**). The structure was solved by molecular replacement, and refined to a maximal resolution of 2.65Å (see methods). The domain boundaries for the human TopIIIα-RMI1 (OB_N) complex are equivalent to that of *S. cerevisiae* Top3-RMI1. Human RMI1 encompasses a DUF1767 three α-helix bundle followed by an N- (OB_N) and C- terminal (OB_C) oligo-nucleotide/saccharide binding domain[17,20] (**fig. 1a, e**). While absent in yeast, OB_C is responsible for RMI2 binding in the human complex [28,29]. RMI2, in turn, recruits the dissolvasome to metazoan repair complexes such as the Fanconi anemia complex[30,31]. Deletion of human RMI1-OB_C has no adverse effect on dHJ dissolution *in vitro* making TopIIIα-BLM-RMI1 (DUF1767+OB_N) the minimal functional dissolvasome complex[29].

Overview of the TopIIIα-RMI1 complex

The overall shape of the TopIIIα–RMI1 complex resembles a brass doorknocker (**fig. 1b**), with TopIIIα forming the ring and RMI1 acting as its base (**fig 1b**). The biological unit was confirmed by single particle

electron microscopy EM as well as mutation witin the heterodimer interface in the asymetric unit (**Supplementary fig. 5** and **fig 1b**).

Human TopIIIα displays the canonical toroidal topoisomerase shape found in all type 1A family members solved to date (**fig 1b**) [32,33,34]. Members of this family comprise five characteristic domains: domain I, or toprim (topoisomerase-primase), harbors an acidic cluster (residues D148, D150 and E152) binding the catalytic metal-ion required for C-strand cleavage[26,35] ; domain II provides the ~26 Å diameter topoisomerase gate formed by two antiparallel topo-fold domains[36]; domains III and IV share similar winged-helix folds (also referred to as catabolite activator protein: CAP)[37,38]; domain III carries the catalytic Tyrosine (Y362) needed for ssDNA cleavage and formation of the 5'-tyrosine *ssDNA* intermediate[27]. The TopIIIα C-terminal region (residues 655 to 1001), also known as domain V, includes a predicted Zinc finger motif (residues 655 to 694). While domains I to IV are well defined in our structure, density for domain V was not unambiguously buildable and has been omitted from the model. No detectable Zn^{2+} anomalous signal was observed that corresponds to domain V (data not shown).

We find that RMI1 *via* its OB_N β-barrel domain attaches to the tip of the TopIIIα topoisomerase gate (domain II) (**fig 1b**). RMI1 binds the toroidal TopIIIα diametric to the toprim ssDNA binding site, with the RMI1 N-terminus projecting away from the topoisomerase. RMI1 attaches to the top of the topoisomerase gate, utilizing an interface frequently used by other OB-fold containing proteins in binding protein ligands, sugars or oligonucleotides[39]. RMI1 injects a large insertion loop, located between β1-β2, into the central gate of the topoisomerase (**fig 1b, Supplementary fig 4a**). This loop, was previously found disordered in the structure of isolated RMI1 where it has been implicated in TopIIIα binding (see below)[29]. The RMI1/TopIIIα arrangement places the RMI1 insertion loop at the center of the topoisomerase gate.

Mechanism of single-strand cleavage

TopIIIα crystalized in the presence of Magnesium (200mM $MgCl_2$), or Calcium (Calcium Citrate 200mM), showed a strong positive f_o-f_c density at the toprim acidic residues cluster (**fig 2a**). We find that Mg^{2+} and Ca^{2+} allow crystallization, and support catalysis[40], while Zn^{2+} or Cs^{2+} were not tolerated in structural studies. Due to the Mg^{2+} dependence of DNA relaxation, the coordination chemistry observed and the proximity of the density to the acidic cluster, we assigned the f_o-f_c density as Mg^{2+} (or Ca^{2+}: for the conditions involving high Calcium concentrations). The metal-ion is *hexa*-coordinated through 5 water molecules and the carboxylic oxygen of E41. The hydroxyl group of Y362 and carboxylic oxygen atoms of E352, D150 provide additional hydrogen bonds to bridging waters within the hydration shell (**fig 2a**). E352, conserved in all eukaryotic orthologues (**fig2b** and **Supplementary fig 2** and **3a**) is not part of the previously identified acidic cluster in *E. coli* topoisomerases, where it is substituted by a glutamine. Other key residues serving comparable roles in eukaryotic and prokaryotic type IA enzymes include: R364 involved in pentavalent phosphate transition-state stabilization, and H414 implicated in anchoring cut ssDNA to the (-1) position[41,42] (**fig. 2b**).

As previous prokaryotic type 1A topoisomerase structures did not show signs of bound catalytic metal ion, the TopIIIα-RMI1 structure now provides insight into type 1A metal mediated ssDNA cleavage: we find one Mg^{2+}/Ca^{2+} ion in our structure, with no indications of further binding sites. Instead, a lysine residues (K42), conserved within the topoisomerase type 1A family (**fig2B**) is situated at the site equivalent to the secondary metal-ion in TopII [43]. K42 is ideally positioned to potentially stabilize the negatively charged pentavalent phosphate transition state arising during trans-esterification, thus serving a functionally equivalent role. Our findings hence favor a one-metal catalytic mechanism also within the type 1A family, as previously proposed[43].

TopIIIα resembles a prokaryotic type1A relaxase

TopIIIα domains I, III and IV share close structural similarity with the Top1A relaxases from *E.coli* and *Thermatoga thermarum* (rmsd: 1.6-1.7 Å over 480 residues, **Supplementary fig. 2** and **3a**), the similarity with the *E.coli* Top3 decatenase is less pronounced (rmsd: 2.7 Å) (**fig 3b**). The most apparent differences between TopIIIα and the prokaryotic Top3 decatenases, however, are the absence of two insertion loops equivalent to *E.coli* 241-255 (*E. coli* Top3 numbering: domain II) and 502-519 (domain IV), both lining the central cavity of the topoisomerase (**fig 3b**). The latter has been implicated in decatenation in the prokaryotic Top3 family (and is henceforth referred to as decatenation loop)[34,44]. Thus TopIIIα, on the structural level, has closer resemblance to a relaxase, not displaying obvious structural features characteristic of prokaryotic type 1A decatenases.

The RMI1-TopIII interface

RMI1 OB_N attaches to the TopIIIα gate acting as the major binding interface occupying a total surface area of 1564.8 $Å^2$. This interface is mainly hydrophobic in nature with acyl chains from RMI1 L177, L181 (β4-β5A loop), V179 (β5A strand), the aromatic ring of Y151 (β3-β4 loop) and methionines M134, M136 and M149 (αI, β2 strand and β3 strands respectively) forming a hydrophobic zipper with TopIIIα L302, L297, V298, L299 and A295 on α12, and L290 on the β10-α12 loop (**fig 1C**). These hydrophobic residues form a hydrophobic groove that accommodates TopIIIα α12. A hydrogen bond network emanating from RMI1 OB_N-domain K78 and R176 (β4-β5A) forms a salt bridge with TopIIIα E305 further stabilizes binding (**fig. 1d**).

The RMI1 insertion loop inserts into the TopIIIα gate

We find that the RMI1 loop, residues 94 to 134, present as an insertion between β9 and β10 lines the gate of the topoisomerase (**fig 1b, 3a**). In the TopIIIα-RMI1 complex, the loop is found in two slightly different conformations. While being less ordered in the presence of Mg^{2+} (**Supplementary fig. 4b**) with

an apparent discontinuity of the electronic density around residues 120 and 131, it can be fully traced in maps obtained from the crystals grown in the presence of Ca^{2+} (**fig. 3a**). The structure obtained in the presence of Ca^{2+} will subsequently be used as a basis for discussion. The RMI1 insertion loop emanates from β1 (D94), and protrudes into the TopIIIα gate creating two layers of aligned and parallel rings (**fig. 1b**). In the conformational state trapped in the crystal, the RMI1 insertion loop restricts the central opening in the TopIIIα gate from 25 Å to 13 Å. As the single stranded DNA has to be moved into the central cavity through an opening between domains I and III, the topoisomerase gate is effectively closed/occupied by the RMI1 loop (**fig. 1b**). Further contacts between RMI1 and TopIIIα are mediated by RMI1 αI, anchoring the loop at three main contact points (**fig. 1e, f**), the majority of which are hydrophobic in nature.

When examining the structure of the TopIIIα–RMI1 complex, we noted that regions where the TopIIIα structure diverges from the *E.coli* Top3 decatenase, RMI1 is found to donate structural motifs *in trans* (**fig. 3a,b**). We therefore focused on the RMI1 insertion loop, examining whether decatenation ability could principally be provided by structural motifs outside the core topoisomerase domain.

The RMI1 insertion loop is required for catenation and dHJ dissolution in vitro

In order to functionally dissect the contribution of the RMI1 insertion loop within the TopIIIα-RMI1 complex *in vivo* and *in vitro*, we switched to yeast as a model system. In comparison to the metazoan RMI1 orthologs, *S. cerevisiae* Rmi1 is more divergent in sequence, whilst retaining the overall domain organization of its metazoan orthologs (DUF1767 + OB_N + loop) (**fig. c** and **Supplementary fig. 3**). The corresponding segment loop is slightly extended spans 58 residues, with little apparent conservation (**fig. 3c**). We first tested whether the *S. cerevisiae* insertion loop can be deleted, or excised using flanking TEV sites. All constructs tested resulted in Rmi1 derivatives with limited solubility and defective Top3 binding (data not shown). We then replaced the 58 amino acid yeast Rmi1 insertion loop (residues D87

to V145) with 23 randomly scrambled residues taken from the human RMI1 loop (**fig. 3c**). This Rmi1 construct, designated randomized loop (rlRmi1), was found proficient in yeast Top3 binding (**Supplementary fig. 6a**) and formed the basis for all subsequent biochemical experiments.

Isolated wild-type Top3 is able to relax negatively supercoiled DNA (scDNA) in presence of Mg^{2+} producing multiple relaxed DNA intermediates on ethidium bromide (EtBr) free gels (**fig. 4a,** - EtBr: compare lanes 1 and 2). Relaxation is inhibited by addition of Rmi1 (lanes 3 to 8). Running gels in the absence of EtBr allows nicked DNA to be chromatographically separated from linear DNA. The subsequent analysis (**fig 4a**, + EtBr: lanes 3 to 8) and quantification (**fig 4b**) revealed a 15-fold increase in the formation of nicked DNA, as a function of wild-type Rmi1 added. Previous work demonstrated that the accumulation of nicked ssDNA species corresponds to Top3 being stabilized in an ssDNA-bound open form, with the scissile phosphate covalently attached to the catalytic tyrosine of domain III[23,24]. When using rlRmi1, however, an increase in nicked DNA, as function of added rlRmi1 was not observed (**fig 4a**, + EtBr: lanes 9 to 14; **fig 4b** for quantification). Intriguingly, gels run without EtBr showed that relaxation is still inhibited in the presence of rlRmi1 (**fig 4a,** - EtBr: lanes 9 to 14), as shown by the progressive loss of the relaxed circular plasmid intermediates.

To rule out that rlRmi1 renders Top3 non-functional in an unspecific fashion, for example through aggregation, we next examined whether Rmi1 also interferes with Top3 mediated single strand cleavage. We reasoned that a potential deleterious effect on Top3 caused by the presence of rlRmi1 would also impair other Top3 mediated reactions, such as single strand cleavage. For this, Top3-rlRmi1 complexes were incubated with circular M13 ssDNA viral DNA at 400nM, the highest Rmi1 concentrations used in relaxation assays (**fig. 4d**). Top3 alone was able to effectively cleave ssDNA into linear intermediates. In the presence of either wild-type or rlRmi1, however, an identical behavior is observed with comparable M13 ssDNA cleavage (**fig. 4d**, **Supplementary fig. 6b**). As judged by single-strand cleavage, rlRmi1 itself is thus not deleterious for Top3 stability. We therefore conclude that

effects on Top3 catalysis observed in the presence of rlRmi1 (**fig 4a**) are likely a direct consequence of loop sequence scrambling and shortening. These experiments demonstrate that the Rmi1 insertion loop is involved in stabilizing Top3 in a nicked, open conformation, while not interfering with the principal ability of Rmi1 to inhibit Top3 mediated relaxation. The insertion loop Rmi1 hence directly influences the open/closing equilibrium of the Top3 gate.

The RMI1 insertion loop is a key element for dHJ dissolution *in vitro*

We next examined the effect of the loop on the catenation/decatenation process. For this purpose concatenation of circular DNA into higher order catenanes was assayed using Top3, *E.coli* single strand binding protein (SSB) and Sgs1 in a reversible reaction previously characterized[23,24]. Catenation required the concerted action of Top3 and Sgs1 in an ATP-dependent reaction. To examine the effect of the Rmi1 insertion loop on catenation, wild-type Rmi1 or rlRmi1 were titrated into the reaction mixture (**fig. 4b**). We observed that wild-type Rmi1 stimulated catenation (lanes 3-6), as evident by the emergence of low velocity migrating species. rlRMI1, on the other hand, did not result in increased formation of catenation products as function of protein added (200 and 400nM) (**fig 4b,** lanes 7-10). The RMI1 insertion loop hence not only influences the opening/closure equilibrium of the topoisomerase, but is also required for catenation/decatenation and will hence subsequently be referred to as decatenation loop.

As catenation is not the presumed biological role of the Top3-Rmi1 complex we next examined the concerted action of Top3 and Sgs1 in dissolution of synthetic double holliday junctions (**fig. 4e**). Wild-type Rmi1 strongly stimulated the dissolution of dHJ by the Top3-Rmi1 complex, resulting in the same amount of radiolabelled dissolution product compared to a control where the dHJ substrate is cleaved by the RsaI restriction enzyme, as previously observed[24,25]. When wild-type Rmi1 is substituted for rlRmi1, the dissolution efficiency is largely impaired yielding similar amounts than that observed in

the absence of Rmi1. This strongly suggests that the decatenation loop and its ability to stabilize the open-state and facilitate catenation/decatenation is also required for dHJ dissolution *in vitro*.

The Rmi1 decatenation loop is required for dissolvasome function *in vivo.*

In order to examine the biological significance of rlRmi1 *in vivo*, we generated a genetically modified yeast strain where the *rmi1* gene has been substituted through a *rlRmi1* version. ΔRmi1 strains exhibit high sensitivity to methyl methanesulfonate (MMS) (**fig. 4f**). MMS forms DNA adducts which in turn give rise to DSBs and activate a HR repair response[45,46]. To avoid accumulation of suppressors, we maintained strains in a diploid state and performed the MMS sensitivity test on freshly dissected tetrad mutant spores. ΔRmi1 strain exhibit slow growth and MMS sensitivity in the presence of 0,012% MMS as described previously [18,22]. Yeast cells having undergone Rmi1 deletion and gene replacement with rlRmi1 show sensitivity at 0,012% MMS exposure similar to that of the ΔRmi1 strain, as well as a slow growth phenotype (**fig. 4f**). This phenotype implies that a defect in the decatenation loop is sufficient to emulate the *ΔRmi1* phenotype and suggests that the decatenation loop is required *in vivo* for dissolution of homologous recombination repair intermediates. In conclusion, the Rmi1 decatenation loop is required for modulating the Top3 open/closure equilibrium and for conversion of Top3 into a decatenating enzyme allowing HJ dissolution, and *in vivo* resolution of otherwise toxic repair intermediates.

Discussion

Type 1A topoisomerases operate in the context of larger macromolecular assemblies. One of the most prominent examples is the eukaryotic topoisomerase III family, responsible for non-crossover dHJ resolution in concert with a dedicated RecQ-type helicase and RMI1. How, on the structural and mechanistic level, topoisomerase action is governed by the toposome, is a key question.

RMI1 injects structural epitope that influences the topoisomerase cycle

We have determined the structure of the human TopIIIα-RMI1(OB_N) complex finding strong resemblance between TopIIIα and a prokaryotic type 1A relaxase. Decatenation is dependent on the RMI1 decatenation loop segment, which is donated *in trans* into the central gate of the topoisomerase. In order to illustrate what may happen in the TopIIIα-RMI1 reaction cycle, we built a TopIIIα model in different stages of decatenation, based on previous structures and normal modes simulations available for *E.coli* Top1A[47,48]. This model depicts domain III and the gate in a presumed open conformation (**fig. 5**), and suggests that gate may create an opening of up to 30 Å in width, analogous to what has been suggested for *E.coli* TopIA[47]. In the presence of RMI1, however, steric hindrance imparted by the mobile part of the RMI1 insertion loop (V116-P131, **fig. 3a**) is expected to restrict gate opening and impact re-closure of the gate. Our biochemical data are consistent with the RMI1 decatenation loop being involved in stabilization of the open state, following nicking of the C-strand (**fig. 5**). By scrambling the sequence and shortening the loop length, we find that the loop is required to maintain the loop in an open conformation. Whether this open state observed biochemically depicts gate opening while single stranded DNA from the T-strand is being accommodated (potentially stabilized by a ssDNA-RMI1 decatenation loop interaction) and/or whether the empty gate is being mainly held open to provide sufficient time to encounter the T-strand which decatenation has to provided in a intra-molecular fashion can not be resolved at present.

It is of note that for the topoisomerase cycle to be completed, the T-strand has to be moved through the C-strand nick, followed by C-strand religation and subsequent T-strand release (**fig. 5**). A certain degree of plasticity within the decatenation loop is thus required to accommodate the single strand DNA upon gate closure, as the cavity between the decatenation loop and the topoisomerase gate only measures around 11 Å at its widest point (with the diameter of ssDNA being approximately 7 Å). This is in line with the plasticity of the decatenation loop observed when comparing the Mg^{2+} and Ca^{2+} crystal forms (**fig. 3a, Supplementary fig. 4b**). In the Mg^{2+} bound structure the loop segment is disordered around the presumed ssDNA T-strand binding site (residues 116 to 131). In the model of the open form we further observe that the pivot region of the gate is in close proximity to the beginning of the decatenation loop (residues P98-Y100) hence providing a potential mechanism of how RMI1 binding could influence the TopIIIα open-close equilibrium. Due to the steric constraint imparted by the presence of the RMI1 decatenation loop with the topoisomase gate, dsDNA accommodation within the TopIIIα gate is unlikely. This is in agreement with the low efficiency (~10 fold) by which dsDNA is accommodated by the Top3-Rmi1 in decatenation experiments[23], and in contrast to the behavior seen in prokaryotic Top3 enzymes[49].

Towards a unified decatenation mechanism of eukaryotic and prokaryotic topoisomerases

The TopIIIα-RMI1 system bears the conceptual advantage that decatenation is dependent on RMI1 addition *in trans*, allowing to directly probe the effect of RMI1 on decatenation, without manipulating the topoisomerase. Prokaryotic type IA topoisomerases implicated in relaxation and those involved in decatenation (e.g.: *E. coli* Top3), share almost identical enzymatic cores with only minimal structural differences, the most significant being the decatenation loop, lining the gate, which is exclusively found in the prokaryotic decatenases[34]. Deletion of this loop in *E.coli* Top3, results in almost complete loss of decatenation, albeit with relaxation also being impaired[44]. The structural equivalent to this loop in the

eukaryotic Top3/TopIIIα decatenases are absent, which has previously been used as an argument against loop mediated decatenation. We now find that RMI1 is inserts a decatenation loop *in trans,* positioned at a similar loci than the prokaryotic decatenation loop. Moreover this loop is required for effective decatenation and dHJ resolution.

Taken together, we propose a model (**fig. 5**) where, following binding and scission of the single strand C-strand, the topoisomerase gate opens. The gate in its open form is stabilized through the RMI1 decatenation loop (or the functionally/structurally equivalent loop found in prokaryotic type IA enzymes). The structure supports a model where the gate in its stabilized cut/open state will provide the toposome with sufficient time to accommodate distant ssDNA T-strands originating from different duplexes (e.g. in dHJ dissolution) moving these strands in/out of the gate, thereby driving decatenation (as an 'inter-molecular process') [23]. In relaxation, on the other hand, where the T-strand belongs to the same duplex as the C-strand (working in an intra-molecular process) movement of DNA strands likely occurs over shorter distances hence not requiring extended gate opening times. While we find that the RMI1 decatenation loop is required for this process, we can exclude that other part of the topoisomerase are involved in the reaction, such as the divergent Top3 C-termini observed in prokaryotes and eukaryotes.

TopIIIα-RMI1 function in the dissolvasome

dHJ dissolution is dependent on the presence of a complete dissolvasome consisting, minimally, of Top3/IIIα, Rmi1/RMI1 and a RecQ helicase. In yeast dissolution, the Sgs1 RecQ helicase serves a catalytic, as well as a non-catalytic scaffolding role. We now find that RMI1 does not fundamentally change the mode of topoisomerase action, but rather modulates its dynamics. In the simplest model (**Supplementary fig. 7**), assuming a 1:1:1 complex of Rmi1/RMI1:Top3/IIIα:Sgs1/BLM (see accompanying paper), the duplex undergoes strand-separation through the helicase, with one strand being guided

through the gate (equivalent to the T-strand position), while the other is being nicked by the topoisomerase around the C-strand. In this manner helicase and topoisomerase action can be coordinated releasing topological strain during branch migration, and the RecQ helicase within the complex can plays a non-catalytic scaffolding effect guiding at least one of the single strand to the C-/T-site of the topoisomerase. Whether a higher order structure exists driving convergent branch migration of two dHJ junctions (likely involving 4 dissolvasome complexes) and what such super-complex may look like is unclear at the moment.

Conclusion

We herein provide molecular insight into the mechanistic influence of the large molecular complex environment, the toposome, on topoisomerase action. It will be exciting to study how other accessory components such RPA, or related complexes such Fanconi and Rif1 do impact on dissolvasome function.

Acknowledgments

This work was supported by the Novartis Research Foundation and grants from Marie Curie Fellowship (FP7-PEOPLE-2009-IEF 253555-TOPO), EMBO long term Fellowship (EMBO ALTF 693-2009), and ERC

We thank Wassim Abdulrahman, Susan Gasser, Ulrich Rass, Kenji Shimada, Jeremy Keush, Eric Fischer, Andrea Scrima, Daniel Hess, Dominique Klein and Martin Renatus for help and fruitful discussion. Part of this work was performed at the Swiss Light Source at the Paul Scherrer Institut, Villigen, Switzerland.

Methods

Protein expression prior crystallization The human TopIIIα (residues 1-753)/RMI1 (residues 1-219) complex is co-expressed in High 5 insect cells using a pFast-Bac vector (Invitrogen). Cells are infected at a 4 million/ml concentration and harvested after 48 hours expression. Lysis (lysis buffer:Tris pH8 50mM, NaCl 200 mM, βMe 1mM, PMSF 1 mM and Sigma Proteases inhibitors cocktail) is performed by sonication followed by clarification of the lysate by ultracentrifugation. Streptactin affinity purification is performed as a first strep affinity step, followed by POROSQ Ion exchange chromatography (Buffers in Tris pH8 50mM and TCEP 0,2 mM) removing traces of endogenous DNA. As a final step, the purified protein was subjected to a size exclusion chromatography on a Superdex 200 column (GE healthcare) (HEPES pH7,4 50mM, NaCl 300mM and TCEP 0,2 mM). Fractions corresponding to a monomeric heterodimer with appropriate ratio are pooled and subjected to further crystallization experiments.

Complex crystallization The complex (8mg/ml) has been crystallized in PEG2000 8-12%, Tris pH7 0,1 M, and $MgCl_2$ 0,2M. Crystals grew only in the presence of Mg^{2+} or Ca^{2+}. The conditions of crystallization for the crystals grown in presence of Ca^{2+} are, Tris pH7.0, 0.1 M, PEG 5k MME 8%, Calcium citrate 0.2 M. Crystals in either Mg^{2+} or Ca^{2+} appeared square based rods growing to maximal dimension within 4-5 days and belong to the tetragonal family ($P4_12_12$ space group) with one heterodimer in the asymmetric unit. Cryopreservation of crystals was performed by supplementation of the mother solution by 35% Ethylene glycol prior flash frozing in liquid nitrogen.

Structure Determination Final datasets have been recorded at the SLS on the PXII beamline (Villigen) at a wavelength of 1.0 Å. Data sets from Mg^{2+} and Ca^{2+} conditions were processed by XDS[50] and the structure solved by molecular replacement using PHASER[51]. An initial search has been made with a

model of *E. coli* Top1A proposed by BALBES server, and sequence optimized by CHAINSAW software[52]. Then a second one with the hRMI1 structure with the top1A as a fixed model.

Refinement. The initial phases have further been refined using a combination of PHENIX[53], REFMAC5[54] and BUSTER[55] software, in addition with TLS constraints. During map inspection, it turns out that the RMI1 insertion loop (residues 116-130) was more ordered and resolved in the Calcium datas although the datas were of a lower average quality (See **Supplementary Table 1**) showing continuous electron density all along the loop allowing unambiguous building. The final refined models (R_{work}/R_{free} (%) for TopIIIα-Mg^{2+} are 20.2/22.6 and for TopIIIα-Ca^{2+}, 20.9/22.8) contains residues RMI 2-216 and TopIIIα 20-637 and one heteroatom of Mg^{2+} or Ca^{2+}, additional pieces of the TopIIIα N- and C-terminus are partially visible but could not be univocally traced and assigned and were omitted from the model. The final Ramachandran statistics are %favoured/%outliers, for TopIIIα-Mg^{2+} (97.1/0) and for TopIIIα-Ca^{2+} (96.1/0.1).

Relaxation, catenation and M13 digest assays with yeast proteins. Yeast Top3, Sgs1 and bacterial SSB are generous gift from Petr Cejka. Yeast Rmi1 wt and rl constructs have been expressed in insect cells (High 5) as GST-Nterm fusion proteins and Cterm His tag following the previously described protocole of lysis to avoid nucleases contamination. Final buffer for protein storage is Tris pH 7.5 50 mM, NaCl 150mM, βMe 1 mM, 10% glycerol. (Final buffer)

For relaxation assay, proteins (Top3 and different RMI1 constructs) are incubated in presence of subtrate PUC19 (200ng per reaction) and incubated 1h at 42°C in a reaction buffer, HEPES pH7.4 25mM, BSA 100μg/ml, Glycerol 32%, NaOc 5mM, MgOAc 0,5mM. The reaction is then stopped by addition of EDTA and Proteinase K for 1hour at 37°C. The samples are loaded on 1% agarose gel poored in presence or not of Ethydium Bromide.

For catenation assay[24], Sgs1 (160nM) and SSB are added in the reaction and the reaction buffer differs as the ATPase activity of Sgs1 is required, Tris pH 7.5 25 mM, MgOAc 1mM, DTT 0.1 mM, Phosphoenol pyruvate 1mM, Pyruvate kinase 80U/ml, BSA 100μg/ml and ATP 1mM. The reactions are incubated at 37°C for 1 hour and stopped as described above.

The M13 (200ng per reaction, M13 mp18 phage ssDNA from Clontech) digest has been done in the same conditions than the relaxation assay. The gel is stained with SYBR green.

Holliday junction dissolution assay. The human RMI1 loop variants have been generated by classical mutagenesis strategy, cloned in pGEX plasmids and produced in *E.coli* ROSETTA strain (OVN expression at 20°C, 0.2mM IPTG). The cells are harvested and lysed by sonification . After ultracentrifugation clarification, a GST sepharose affinity strep is performed followed by a OVN TEV cleavage (4°C, 2% of TEV protease). RMI1 protein is further purified by a POROS Q ion exchange chromatography allowing the separation of GST tag (elution around 140mM salt) from RMI1 (elution around 200mM). The proteins are then dialysed overnight against final buffer.

Yeast strain generation and drug sensitivity test.

Δ*Rmi1* and *Rmi1rl* strains have been 2 times backcrossed with the yeast WT303. The obtained mutants clones were mated with the WT303 and big diploid colonies were selected and placed on a sporulation plates. 5 to 10 tetrads were dissected and smaller clones were picked for MMS test.
O/N cultures from the smaller colonies were diluted to OD600 = 0.5 and grow for 4h at 37°C. The ODs were set to 0.1 and step diluted (1/10) 5 times. YPAD + MMS 0.012% plates were freshly prepared and dried 15 min at 37°C. 4 ml drops of each dilution are plated. The plate are placed at 30°C for 48h.

References

1. Petermann, E. & Helleday, T. Pathways of mammalian replication fork restart. *Nature reviews. Molecular cell biology* **11**, 683-7 (2010).
2. Moynahan, M.E. & Jasin, M. Mitotic homologous recombination maintains genomic stability and suppresses tumorigenesis. *Nature reviews. Molecular cell biology* **11**, 196-207 (2010).
3. Holliday, R. A mechanism for gene conversion in fungi. *Genetical research* **89**, 285-307 (2007).
4. Szostak, J.W., Orr-Weaver, T.L., Rothstein, R.J. & Stahl, F.W. The double-strand-break repair model for recombination. *Cell* **33**, 25-35 (1983).
5. Heyer, W.D., Ehmsen, K.T. & Solinger, J.A. Holliday junctions in the eukaryotic nucleus: resolution in sight? *Trends in biochemical sciences* **28**, 548-57 (2003).
6. Matos, J., Blanco, M.G., Maslen, S., Skehel, J.M. & West, S.C. Regulatory control of the resolution of DNA recombination intermediates during meiosis and mitosis. *Cell* **147**, 158-72 (2011).
7. Heyer, W.D. Recombination: Holliday junction resolution and crossover formation. *Current biology : CB* **14**, R56-8 (2004).
8. Cavenee, W.K. et al. Expression of recessive alleles by chromosomal mechanisms in retinoblastoma. *Nature* **305**, 779-84 (1983).
9. Thiagalingam, S. et al. Mechanisms underlying losses of heterozygosity in human colorectal cancers. *Proceedings of the National Academy of Sciences of the United States of America* **98**, 2698-702 (2001).
10. LaRocque, J.R. et al. Interhomolog recombination and loss of heterozygosity in wild-type and Bloom syndrome helicase (BLM)-deficient mammalian cells. *Proceedings of the National Academy of Sciences of the United States of America* **108**, 11971-6 (2011).
11. Wu, L. & Hickson, I.D. The Bloom's syndrome helicase suppresses crossing over during homologous recombination. *Nature* **426**, 870-4 (2003).
12. Gangloff, S., McDonald, J.P., Bendixen, C., Arthur, L. & Rothstein, R. The yeast type I topoisomerase Top3 interacts with Sgs1, a DNA helicase homolog: a potential eukaryotic reverse gyrase. *Molecular and cellular biology* **14**, 8391-8 (1994).
13. Bennett, R.J., Noirot-Gros, M.F. & Wang, J.C. Interaction between yeast sgs1 helicase and DNA topoisomerase III. *The Journal of biological chemistry* **275**, 26898-905 (2000).
14. Fricke, W.M., Kaliraman, V. & Brill, S.J. Mapping the DNA topoisomerase III binding domain of the Sgs1 DNA helicase. *The Journal of biological chemistry* **276**, 8848-55 (2001).
15. Harmon, F.G., DiGate, R.J. & Kowalczykowski, S.C. RecQ helicase and topoisomerase III comprise a novel DNA strand passage function: a conserved mechanism for control of DNA recombination. *Molecular cell* **3**, 611-20 (1999).
16. Cejka, P. & Kowalczykowski, S.C. The full-length Saccharomyces cerevisiae Sgs1 protein is a vigorous DNA helicase that preferentially unwinds holliday junctions. *The Journal of biological chemistry* **285**, 8290-301 (2010).
17. Xu, D. et al. RMI, a new OB-fold complex essential for Bloom syndrome protein to maintain genome stability. *Genes & development* **22**, 2843-55 (2008).
18. Mullen, J.R., Nallaseth, F.S., Lan, Y.Q., Slagle, C.E. & Brill, S.J. Yeast Rmi1/Nce4 controls genome stability as a subunit of the Sgs1-Top3 complex. *Molecular and cellular biology* **25**, 4476-87 (2005).
19. Singh, T.R. et al. BLAP18/RMI2, a novel OB-fold-containing protein, is an essential component of the Bloom helicase-double Holliday junction dissolvasome. *Genes & development* **22**, 2856-68 (2008).
20. Raynard, S., Bussen, W. & Sung, P. A double Holliday junction dissolvasome comprising BLM, topoisomerase IIIalpha, and BLAP75. *The Journal of biological chemistry* **281**, 13861-4 (2006).

21. Lai, M.S., Seki, M., Ui, A. & Enomoto, T. Rmi1, a member of the Sgs1-Top3 complex in budding yeast, contributes to sister chromatid cohesion. *EMBO reports* **8**, 685-90 (2007).
22. Chang, M. et al. RMI1/NCE4, a suppressor of genome instability, encodes a member of the RecQ helicase/Topo III complex. *The EMBO journal* **24**, 2024-33 (2005).
23. Cejka, P., Plank, J.L., Dombrowski, C.C. & Kowalczykowski, S.C. Decatenation of DNA by the S. cerevisiae Sgs1-Top3-Rmi1 and RPA complex: a mechanism for disentangling chromosomes. *Molecular cell* **47**, 886-96 (2012).
24. Cejka, P., Plank, J.L., Bachrati, C.Z., Hickson, I.D. & Kowalczykowski, S.C. Rmi1 stimulates decatenation of double Holliday junctions during dissolution by Sgs1-Top3. *Nature structural & molecular biology* **17**, 1377-82 (2010).
25. Chen, C.F. & Brill, S.J. Binding and activation of DNA topoisomerase III by the Rmi1 subunit. *The Journal of biological chemistry* **282**, 28971-9 (2007).
26. Corbett, K.D. & Berger, J.M. Structure, molecular mechanisms, and evolutionary relationships in DNA topoisomerases. *Annual review of biophysics and biomolecular structure* **33**, 95-118 (2004).
27. Tse, Y.C., Kirkegaard, K. & Wang, J.C. Covalent bonds between protein and DNA. Formation of phosphotyrosine linkage between certain DNA topoisomerases and DNA. *The Journal of biological chemistry* **255**, 5560-5 (1980).
28. Hoadley, K.A. et al. Structure and cellular roles of the RMI core complex from the bloom syndrome dissolvasome. *Structure* **18**, 1149-58 (2010).
29. Wang, F. et al. Crystal structures of RMI1 and RMI2, two OB-fold regulatory subunits of the BLM complex. *Structure* **18**, 1159-70 (2010).
30. Hoadley, K.A. et al. Defining the molecular interface that connects the Fanconi anemia protein FANCM to the Bloom syndrome dissolvasome. *Proceedings of the National Academy of Sciences of the United States of America* **109**, 4437-42 (2012).
31. Deans, A.J. & West, S.C. FANCM connects the genome instability disorders Bloom's Syndrome and Fanconi Anemia. *Molecular cell* **36**, 943-53 (2009).
32. Lima, C.D., Wang, J.C. & Mondragon, A. Three-dimensional structure of the 67K N-terminal fragment of E. coli DNA topoisomerase I. *Nature* **367**, 138-46 (1994).
33. Hansen, G., Harrenga, A., Wieland, B., Schomburg, D. & Reinemer, P. Crystal structure of full length topoisomerase I from Thermotoga maritima. *Journal of molecular biology* **358**, 1328-40 (2006).
34. Mondragon, A. & DiGate, R. The structure of Escherichia coli DNA topoisomerase III. *Structure* **7**, 1373-83 (1999).
35. Aravind, L., Leipe, D.D. & Koonin, E.V. Toprim--a conserved catalytic domain in type IA and II topoisomerases, DnaG-type primases, OLD family nucleases and RecR proteins. *Nucleic acids research* **26**, 4205-13 (1998).
36. Duguet, M., Serre, M.C. & Bouthier de La Tour, C. A universal type IA topoisomerase fold. *Journal of molecular biology* **359**, 805-12 (2006).
37. Schultz, S.C., Shields, G.C. & Steitz, T.A. Crystal structure of a CAP-DNA complex: the DNA is bent by 90 degrees. *Science* **253**, 1001-7 (1991).
38. Brennan, R.G. & Matthews, B.W. The helix-turn-helix DNA binding motif. *The Journal of biological chemistry* **264**, 1903-6 (1989).
39. Flynn, R.L. & Zou, L. Oligonucleotide/oligosaccharide-binding fold proteins: a growing family of genome guardians. *Critical reviews in biochemistry and molecular biology* **45**, 266-75 (2010).
40. Goulaouic, H. et al. Purification and characterization of human DNA topoisomerase IIIalpha. *Nucleic acids research* **27**, 2443-50 (1999).
41. Changela, A., DiGate, R.J. & Mondragon, A. Crystal structure of a complex of a type IA DNA topoisomerase with a single-stranded DNA molecule. *Nature* **411**, 1077-81 (2001).

42. Changela, A., DiGate, R.J. & Mondragon, A. Structural studies of E. coli topoisomerase III-DNA complexes reveal a novel type IA topoisomerase-DNA conformational intermediate. *Journal of molecular biology* **368**, 105-18 (2007).
43. Schmidt, B.H., Burgin, A.B., Deweese, J.E., Osheroff, N. & Berger, J.M. A novel and unified two-metal mechanism for DNA cleavage by type II and IA topoisomerases. *Nature* **465**, 641-4 (2010).
44. Li, Z., Mondragon, A., Hiasa, H., Marians, K.J. & DiGate, R.J. Identification of a unique domain essential for Escherichia coli DNA topoisomerase III-catalysed decatenation of replication intermediates. *Molecular microbiology* **35**, 888-95 (2000).
45. Beranek, D.T. Distribution of methyl and ethyl adducts following alkylation with monofunctional alkylating agents. *Mutation research* **231**, 11-30 (1990).
46. Krogh, B.O. & Symington, L.S. Recombination proteins in yeast. *Annual review of genetics* **38**, 233-71 (2004).
47. Feinberg, H., Lima, C.D. & Mondragon, A. Conformational changes in E. coli DNA topoisomerase I. *Nature structural biology* **6**, 918-22 (1999).
48. Xiong, B. et al. The type IA topoisomerase catalytic cycle: A normal mode analysis and molecular dynamics simulation. *Proteins* **71**, 1984-94 (2008).
49. Li, Z., Mondragon, A. & DiGate, R.J. The mechanism of type IA topoisomerase-mediated DNA topological transformations. *Molecular cell* **7**, 301-7 (2001).
50. Kabsch, W. Automatic Processing of Rotation Diffraction Data from Crystals of Initially Unknown Symmetry and Cell Constants. *Journal of Applied Crystallography* **26**, 795-800 (1993).
51. Mccoy, A.J. et al. Phaser crystallographic software. *Journal of Applied Crystallography* **40**, 658-674 (2007).
52. Stein, N. CHAINSAW: a program for mutating pdb files used as templates in molecular replacement. *Journal of Applied Crystallography* **41**, 641-643 (2008).
53. Adams, P.D. et al. PHENIX: a comprehensive Python-based system for macromolecular structure solution. *Acta Crystallographica Section D-Biological Crystallography* **66**, 213-221 (2010).
54. Murshudov, G.N., Vagin, A.A. & Dodson, E.J. Refinement of macromolecular structures by the maximum-likelihood method. *Acta Crystallographica Section D-Biological Crystallography* **53**, 240-255 (1997).
55. G., B. et al. BUSTER version X.Y.Z. *Cambridge, United Kingdom: Global Phasing Ltd.*

(2011).

Figure 1. Overall architecture and TopIIIα/RMI1 binding interface

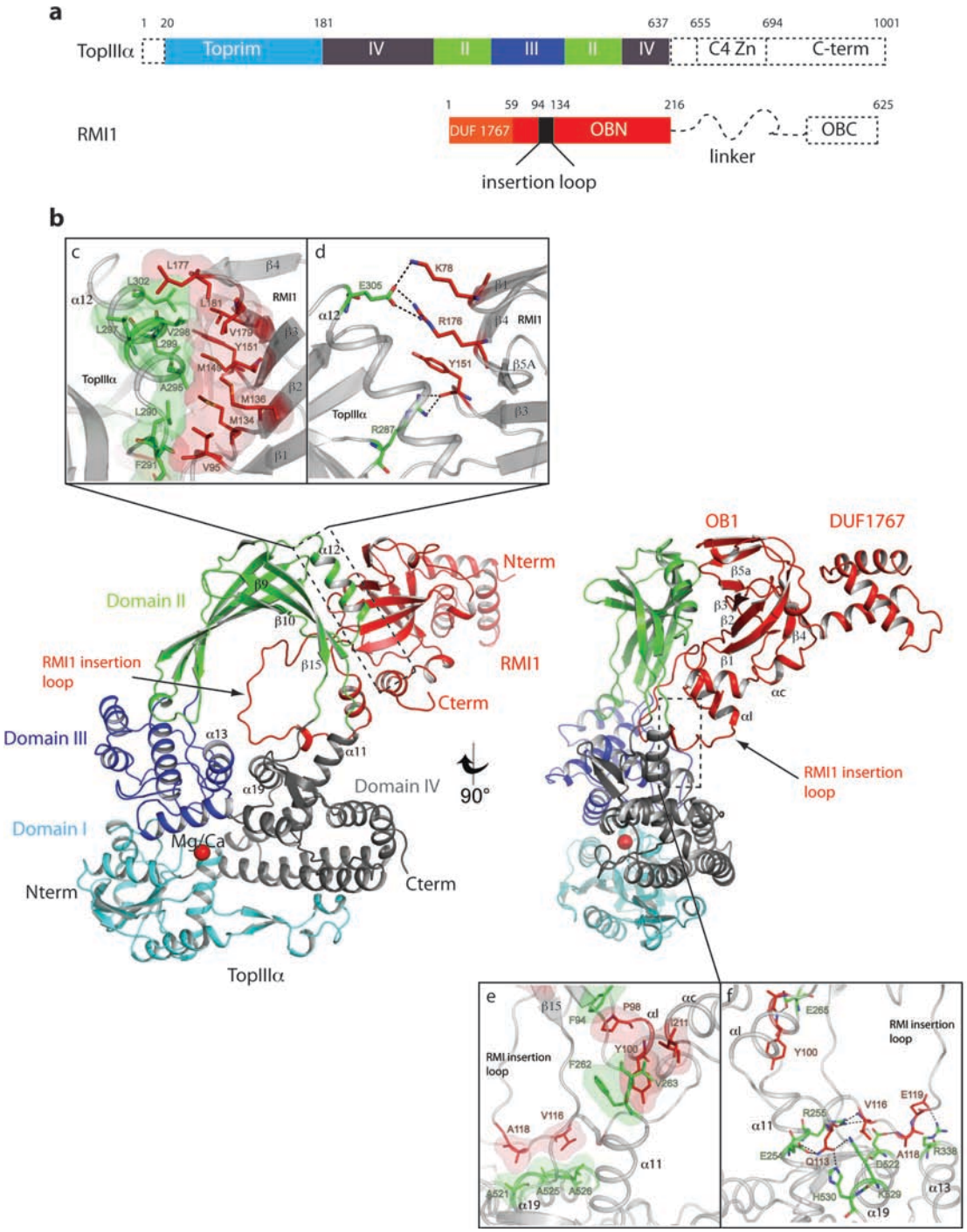

Fig 1 a) Domain organisation of the human TopIIIα / RMI1 complex. The dashed region are not included in the final model (see methods) b) Overall architecture of the crystallized complexe (pdb from Ca). Toprim domain (I) is in cyan; the gate domain (II) with the two topo fold domain in green; catalytic 5Y-CAP domain (III) in blue, and non catalytic CAP domain (IV) in grey. RMI1 is in red. The ion binding site in the catalytic site is represented as a red sphere. The four smaller inserts show the spread interaction network between RMI1 and TopIIIα. c) Hydrophobic zipper between residues from OB domain (belonging to β1, β2, β3 and β5A strands as well as to insertion, β3-β4, and β4-β5A loops) of RMI1 and residues belonging to α12 and β10-α12 loop of TopIIIα. d) Hydrogen bonding network between residues of α3-β1, β4-β5A and β3-β4 RMI1 loops and residues of TopIII α α12 and β10-α12 loop. TopIIIα E305 and RMI1 R176 create a salt bridge. e) Hydrophobic patch clamping the bottom of the RMI1 insertion loop to the TopIIIα α19 helix. An additional zone of hydrophobic contacts is shown between TopIIIα α11-β9 loop and the beginning of RMI1 αI as well as I211 from RMI1 αC helix. P98 creates a stacking interaction with TopIIIα F94 as well as Y100 with TopIIIα F262. In this region I211 from αC interacts with V263 maintaining the RMI1 C terminus close to the beginning of αI. At the top of the TopIIIα Domain IV on α19, A118 and V116 interact hydrophobically with A521, A525 and A526. f) Hydrogen bonding network in the same area described than in e panel. A ionic interaction between RMI1 E119 and TopIIIα R338 contributes to hold the RMI1 insertion loop in this position. RMI1 Q113 is at the center of a hydrogen bonding network involving the oxygen of the carboxylic group of TopIIIα α11 E254 as well as the imidazol group of H530 and the ε-amino group of K529.

Figure 2 Topoisomerase III α catalytic site.

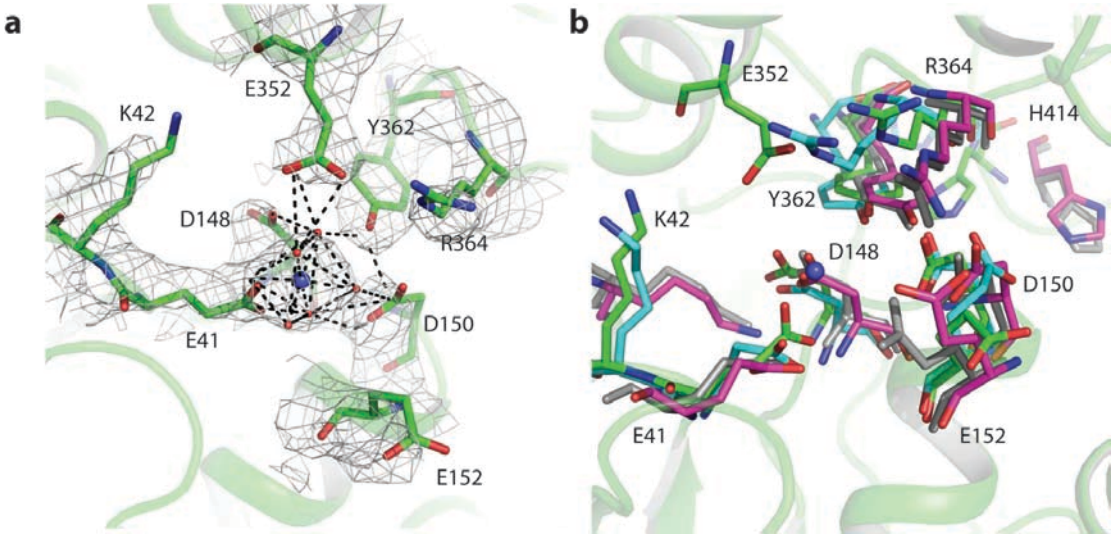

Fig2. Catalytic site of human TopIIIα. a) catalytic site residues and Mg^{2+} binding site. 2fo-fc map is contoured at 1.5σ. Mg^{2+} is represented as a blue sphere and water molecules from the coordination shell as red spheres. Polar contacts are represented as dashed black lines. E41 is the sole residue directly contacting the Mg^{2+} ion while Y362, D150 and E352 bridge the water molecules. b) Structural alignement of the different catalytic sites from crystallised topoisomerases from the 1A family. Cyan is *E. coli* Top3 in apo state (pdb 1D6M), magenta is *E. coli* Top1A in apo state (pdb 1ECL), grey is Top1A from *Thermotoga maritima* (pdb 2GAI), in green the human TopIIIα described in this paper (pdb with Mg^{2+}).

Figure 3: The RMI1 decatenation loop

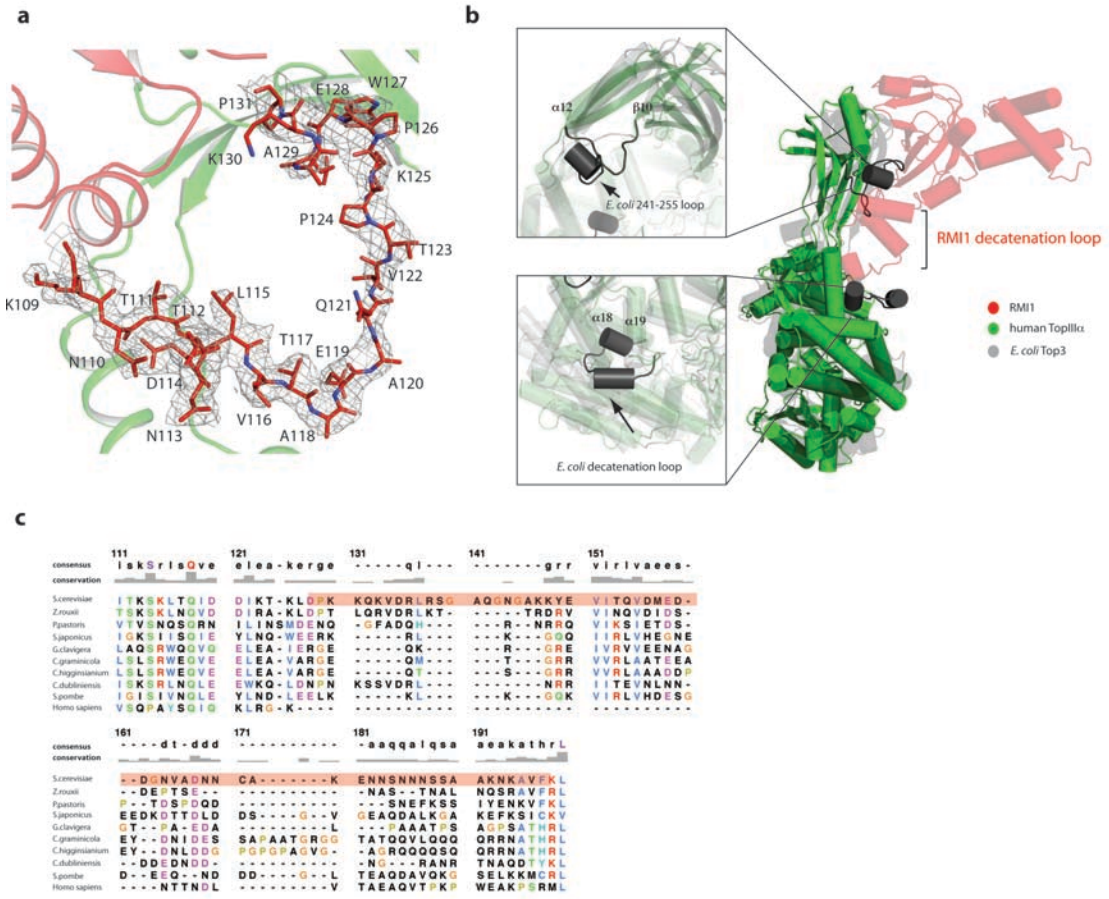

Fig3. a) Final model of the RMI1 decatenation loop. 2fo-fc map is contoured at 1σ. b) Comparison between *E. coli* Top3 (shaded grey) and human TopIIIα (green). RMI1 (shaded red) inserts motifs where *E. coli* Top3 diverges from human TopIIIα. c) Sequence alignements between different yeast strains and the human RMI1 protein at the bottom of the alignement. The shaded region on the *S. cerevisiae* sequence is the region which has been randomized in the rlRmi1 construct (see Methods).

Figure 4. The yeast RMI1 decatenation loop stabilizes the Top3 open form and stimulates dissolution of dHJ

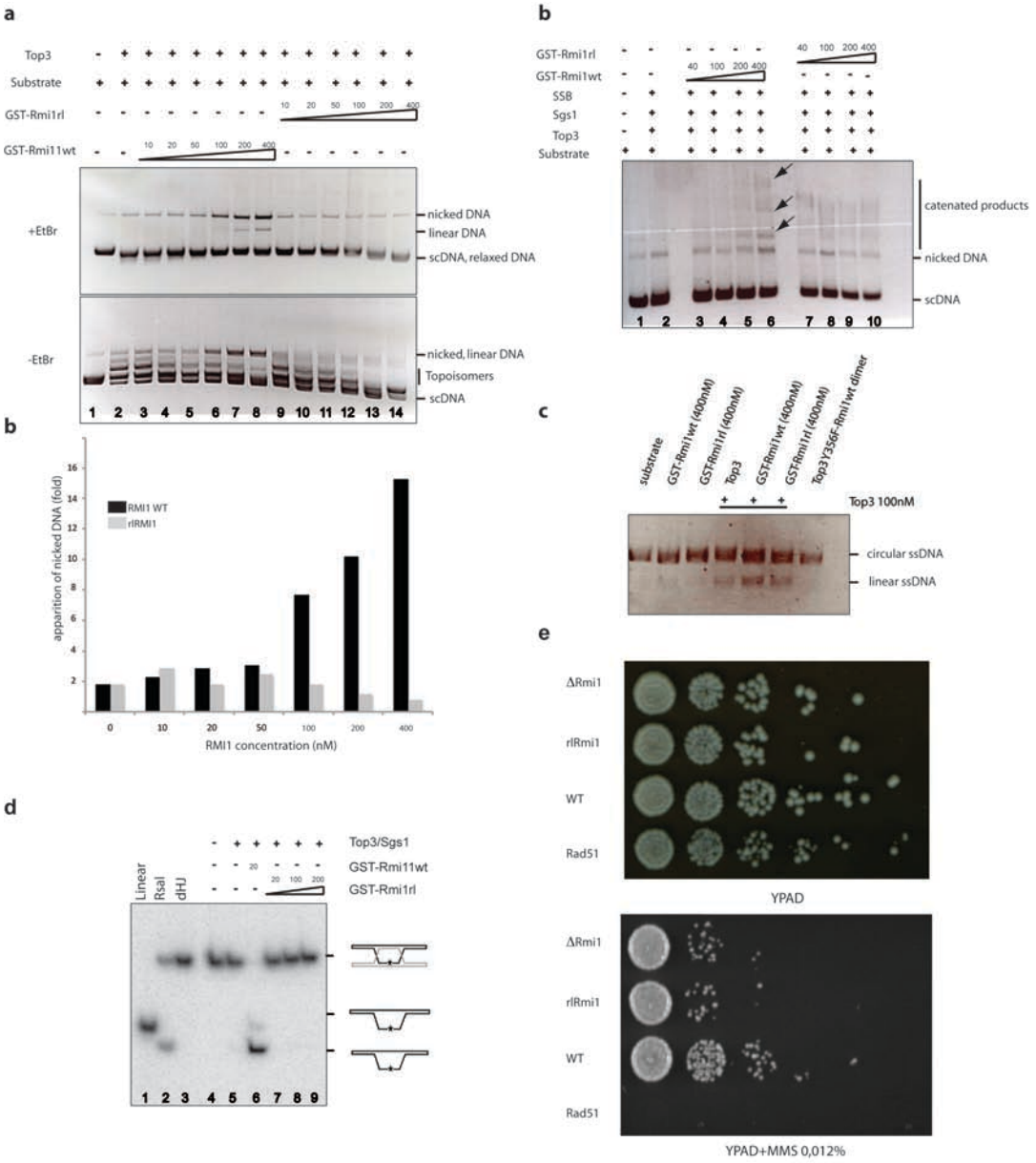

Fig 4 a) Relaxation assay comparing yeast Rmi1 wild type and rlRmi1. Lane 1 is the substrate (PUC19) alone; Lane 2 is the relaxation activity of yeast Top3; Lanes 3-8, increasing concentrations of wtRmi1 and Lanes 8 to 14 are rlRmi1 titration. The same samples are run on 1% agarose gels containing EtBr or not to discriminate linear DNA from nicked DNA (see methods). b) The graph represents the densitometric analysis of the nicked DNA band intensity for WT (grey) and rl (black) on the EtBr gel. c) Catenation of PUC19 substrate by the *in vitro* reconstituted yeast bloom complex with wild type Rmi1 (Lanes 3 to 6) and rlRmi1 (lanes 7 to 10). The appearing catenated products are signalled with a black arrow. d) Digest of M13 substrate with the different complexes used in relaxation and catenation assays. Y356F Top3 mutant is catalytically inactive. e) Dissolution assay on the yeast proteins. The dissolution in presence of wtRmi1 is strongly stimulated as shown by the increased amount of dissolution product. In the presence of rlRmi1, the level of dissolution returns at the basal activity seen in the absence of Rmi1. f) MMS sensitivity drop assay on rlRmi1 yeast strain. The different haploid strains are plated in 1:10 serial dilutions on YPAD ± MMS 0.012%. The rlRmi1 and ΔRmi1 show the same sensitivity to MMS, one order of magnitude higher than for the WT.

Figure 5. Proposed decatenation model by Top3α-RMI1 complex

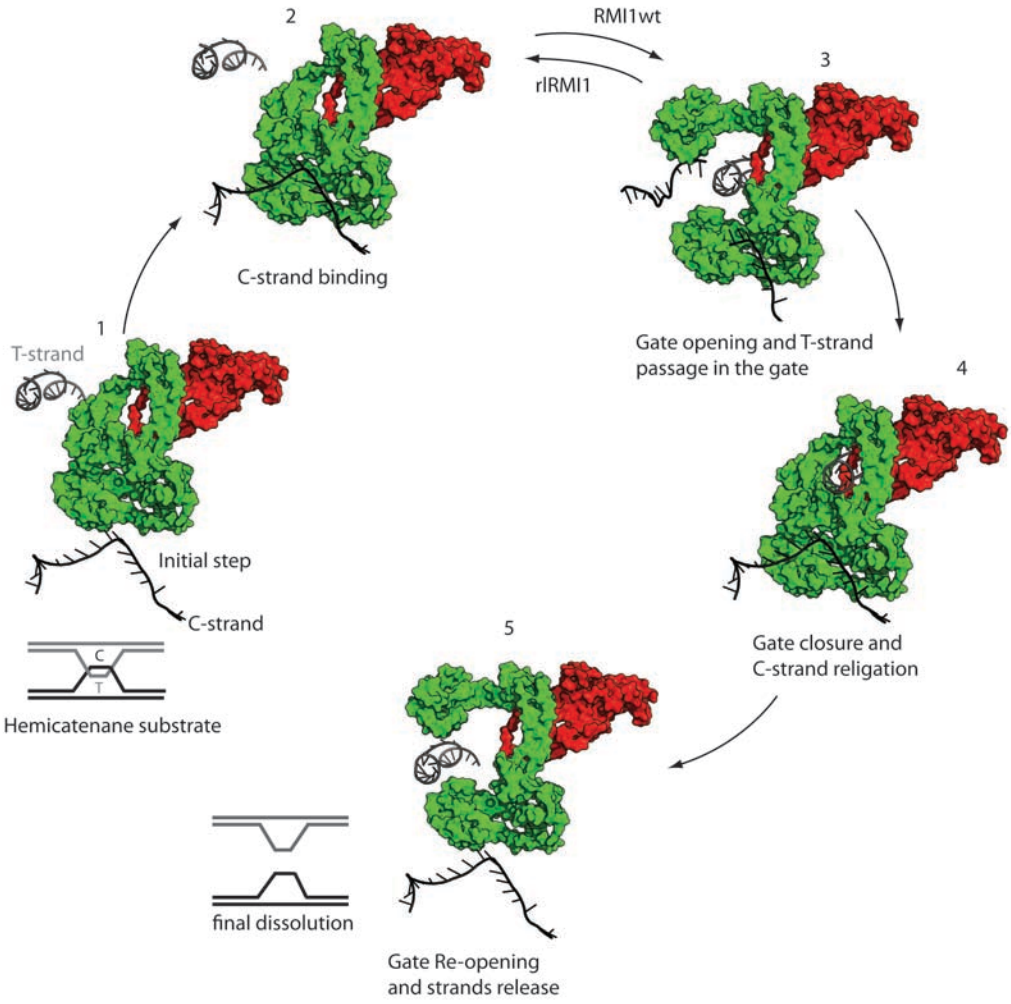

Fig5. Role of RMI1 decatenation loop in hemicatenane dissolution. To decatenate and, by extension, to dissolve dHJ intermediates, TopIIIα (in green) has first to load on hemicatenane substrate and nick the C-strand (in black) (step 2) bound in the catalytic site in order to create a gap through which the T-strand (in grey) can be passed. The strand passage step (step 3) can be then achieved following the opening of the TopIIIα gate. RMI1 (in red) wild type stabilizes this step by favouring the TopIIIα open form while the rlRMI1 construct will displace the equilibrium towards the closed form disfavouring the strand passage *in trans.* Once the T-strand is inside the gate, the latter re-closes to religate the C-strand, trapping the T-strand (step 4). The steric crowding of the gate by the RMI1 decatenation loop exclusively allows ssDNA to be catalysed by the complex and to be passed through the gate. Step 5 corresponds to the final release of the C and T strands by re-opening of the gate ending in disentanglement of the two DNA molecules. The complex finally comes back under its unbound state where it will be able to decatenate another substrate.